

Article

A Novel Prognostic Model of the Degradation Malfunction Combining a Dynamic Updated-ARIMA and Multivariate Isolation Forest: Application to Radar Transmitter

Yuting Zhai ^{1,2} , Dongli Liu ², Zhanxin Cheng ² and Shaojun Fang ^{1,*} 

¹ Department of Information Science and Technology, Dalian Maritime University, Dalian 116026, China; zhaiyt0603@126.com

² Department of Information Systems, Dalian Naval Academy, Dalian 116018, China; 18904284999@126.com (D.L.); czxiaobai@163.com (Z.C.)

* Correspondence: fangshj@dlmu.edu.cn

Abstract: In the prognosis of radar transmitter degradation malfunction, there are some restrictions, such as the fact that it is difficult to obtain fault samples and the monitoring data cannot reach the fault threshold. For these restrictions, a novel data-driven prognostic method is proposed to predict the radar transmitter degradation malfunction, in which the dynamic updated-auto-regressive integrated moving average is proposed to be used to predict the subsequent time-step of the microwave measurement historical data, and the multivariate isolation forest established without fault samples is used to detect the degradation malfunction. The validity and portability of the model are verified using two-type of degradation malfunction prognostic experiments. The experimental results show that the degradation malfunction can be predicted at least 10 time-steps (100 min) before the occurrence of a degradation malfunction. Compared with the existing radar degradation malfunction prediction methods, the proposed method needs less historical data, no fault samples, no artificial thresholds, and no extracting features. This method can complete a degradation malfunction prognosis when there are relevant restrictions.

Keywords: fault prognosis; degradation malfunction; radar transmitter; artificial intelligence



Citation: Zhai, Y.; Liu, D.; Cheng, Z.; Fang, S. A Novel Prognostic Model of the Degradation Malfunction Combining a Dynamic Updated-ARIMA and Multivariate Isolation Forest: Application to Radar Transmitter. *Electronics* **2022**, *11*, 1921. <https://doi.org/10.3390/electronics11121921>

Academic Editor: Anna Richelli

Received: 1 June 2022

Accepted: 19 June 2022

Published: 20 June 2022

Publisher's Note: MDPI stays neutral with regard to jurisdictional claims in published maps and institutional affiliations.



Copyright: © 2022 by the authors. Licensee MDPI, Basel, Switzerland. This article is an open access article distributed under the terms and conditions of the Creative Commons Attribution (CC BY) license (<https://creativecommons.org/licenses/by/4.0/>).

1. Introduction

For marine radar, the radar transmitter is regarded as the heart of the radar and is a component with frequent failures. The degradation of the transmitter's performance will weaken its radar detection capabilities and seriously affect the quality of navigation and related tasks. Once the transmitter undergoes the degradation malfunction during sailing, it will cause unpredictable consequences. However, the current prognosis of radar degradation malfunction mainly relies on manual routine maintenance before fault and built-in test (BIT) warnings when a fault occurs. However, the former requires a lot of manpower and time, and the latter cannot meet the actual demand for early warning of degradation malfunctions. In recent years, with the rapid development of sensors and microwave measurement technology, the historical working data of the system can be collected using sensors or microwave measurement technology, and the working status of the system can be predicted or managed by various intelligent algorithms and data models. Although these technologies can effectively solve the abovementioned problems, as the complexity of marine radar systems continues to increase, there are more and more restrictions for the prognosis of radar transmitter degradation malfunctions based on microwave measurements. On the one hand, the monitoring data fluctuate within the normal range before the occurrence of the degradation malfunction, and the data do not obey a specific mathematical distribution, so they are unable to effectively set the degradation malfunction threshold. On the other hand, the correlation between the historical data collected by each

microwave measurement point is unknown, and the number of fault samples that can be monitored is extremely limited (or even zero). Therefore, how to realize the prognosis of the degradation malfunction of the radar transmitter in the face of the mentioned restrictions has become an urgent problem to be solved.

The research to date has tended to focus on prognostic methods based on measurement and data-driven models, which have been widely used in transportation [1–3], biology [4,5], machinery [6–8], energy [9–11], market [12–14], radar [15–24], and other applications. Among them, the research results of malfunction prognoses in radar-related fields continue to emerge. Zhang et al. [15] established the relationship between the signal subspace to identify the fault of the antenna. Khan et al. [16] proposed a simple method to diagnose the position of the damaged sensors for a linear array antenna using the symmetrical sensor damaged technique and the radiation pattern. Chen et al. [17] adopted the fault-prediction method based on entropy values to predict the array antenna fault of bistatic multiple-input–multiple-output (MIMO) radar. Finchera et al. [18] realized the online failure detection of large massive MIMO linear arrays utilizing numerical optimization of the position of a few near-field probes. Liu et al. [19] established the function between predicted data and historical data to calculate the radar’s remaining useful life using the prediction method of the non-parametric regression kernel function. Li et al. [20] used a diagnosis model with a dynamic threshold based on deep learning to predict the meteorological radar fault. Zhai et al. [21] proposed a prediction model combining the multivariate long short-term memory (LSTM) networks with a multivariate Gaussian distribution to predict the transmitter degradation fault. Wang et al. [22] developed a data-driven fault-detection method using principal component analysis to detect the fault of the fans in a radar cooling system. Li et al. [23] achieved the classification of radar equipment faults utilizing a data-augmentation method based on TF-IDF features. Zhao et al. [24] presented a testable radar system design and demonstration approach based on fault modes and software control actions for improving the self-diagnosis ability of a radar system and reducing the fault rate. Unfortunately, there are many limitations in the above radar-malfunction prognosis methods. These are shown in Table 1. It can be seen from the table, References [15–18,22,23] needed to extract the effective feature or radiation pattern of the degradation fault. In [19,22], an artificial threshold needed to be set to judge the fault. Reference [19,20,23,24] also needed extensive historical data and fault samples for its training sets. Although reference [21] solves the two restrictions of radar transmitter degradation fault, this method is not accurate enough for data prediction, and at least one fault sample is still needed.

Table 1. The limitations in the existing radar malfunction prognosis methods.

The Limitations	Reference
Feature extraction required	[15–18,22,23]
Artificial threshold required	[19,22]
Extensive historical data and fault samples required	[19,20,23,24]

By analyzing the constraints of the fault-prediction model in Table 1, it can be seen that the need for building a radar transmitter degradation malfunction prognosis model that using less historical data, no artificial thresholds, no features extraction, and no fault samples is urgent. To meet the above requirements, a novel prognostic model combined with dynamic updated-auto-regressive integrated moving average (DU-ARIMA) and multiple isolation forest (M-iForest) is proposed for radar transmitter degradation malfunction. The main contributions of this article can be summarized as follows:

- (1) A novel radar transmitter degradation malfunction prognosis model is proposed.
- (2) The accuracy of the future time-step for monitoring data prediction is improved.

- (3) Radar transmitter degradation malfunction detection is realized when there are small samples, no fault samples, no feature extractions, and no artificial thresholds.

The paper is organized as follows: Section 2 analyzes the proposed prognostic model theoretically. The experiment in Section 3 verifies the feasibility and portability of the model. Section 4 provides the conclusions.

2. Prognostic Model of Radar Transmitter Degradation Malfunction

The proposed radar transmitter degradation fault prognosis model combines the advantages of DU-ARIMA and M-iForest. A flow chart of the model is shown in Figure 1. The model consists of three steps. Step 1: microwave measurement and data pre-processing. Step 2: the adoption of DU-ARIMA for data forecasting. Step 3: the M-iForest model to detect the degradation malfunction.

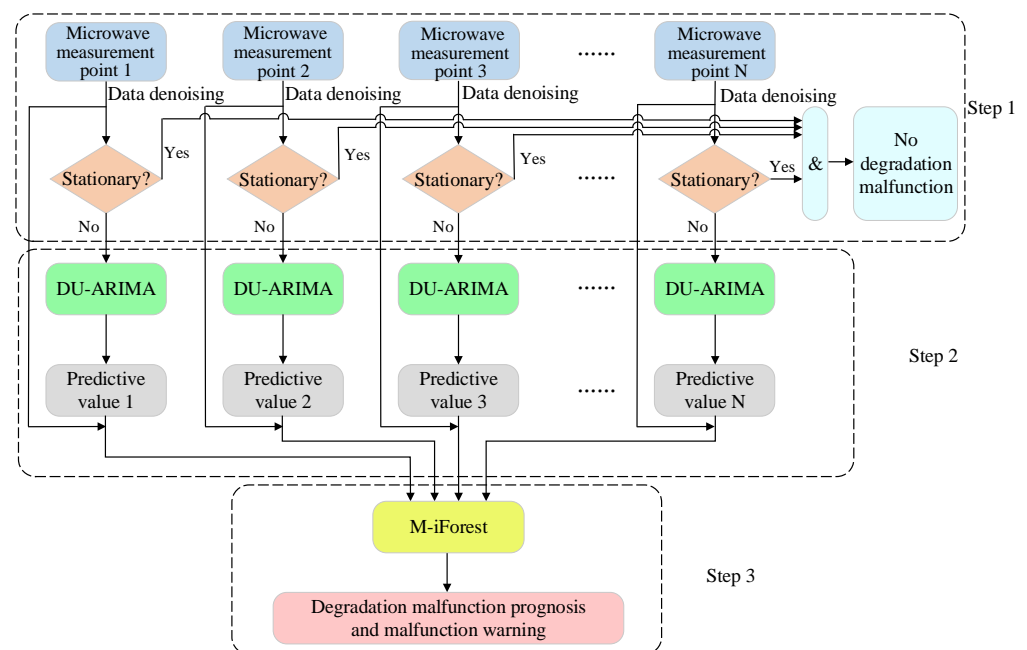


Figure 1. The flow chart of the degradation malfunction prognosis model.

2.1. Microwave Measurement and Data Pre-Processing

The experimental data is collected by microwave measurement performed on a certain type of marine radar transmitter. There is noise in the measurement data, and, therefore, it is necessary to pre-process the measurement data. The classic wavelet threshold denoising method [25] is selected in the proposed model. The parameter settings include: the threshold function is a soft threshold, the threshold is a heuristic threshold, the wavelet decomposition level is 1, and the wavelet base is Daubechies (db4).

The next pre-processing step is the stationarity test. It is used to test the stability of the measured data at each microwave-measuring point. The model chooses two commonly used and complementary stationarity test methods, Augmented Dickey–Fuller (ADF) [26] and Kwiatkowski–Phillips–Schmidt–Shin (KPSS) [27]. Among them, only when the return value of ADF is 1 and the KPSS is 0, is the historical measurement data a stationary series, while the rest of the return values are judged to be non-stationary series. If the historical data of each microwave measurement point is a stationary series, it indicates that the transmitter has no degradation malfunction. Otherwise, it is necessary to predict the subsequent time-steps of the measurement data to determine whether there is a degradation malfunction.

2.2. Dynamically Updated-Auto-Regressive Integrated Moving Average

After data pre-processing, it is necessary to predict the subsequent time-step of the historical data. To improve the accuracy of the data prediction, the DU-ARIMA method is proposed. DU-ARIMA is an improved auto-regressive integrated moving average (ARIMA) designed to improve the prediction accuracy of ARIMA [28]. The DU-ARIMA(p, d, q) model can be expressed as

$$\begin{aligned} &\Phi(B)(1 - B)^d x_t = \Theta(B)\varepsilon_t, \\ \text{s.t. } &E(\varepsilon_t) = 0, \text{Var}(\varepsilon_t) = \sigma_\varepsilon^2, E(\varepsilon_t \varepsilon_s) = 0, s \neq t, \\ &E(x_s \varepsilon_t) = 0, \forall s < t, d > 0, \\ &x_{t+1} \text{ can be dynamically updated,} \end{aligned} \tag{1}$$

where x_t is the current time-series, ε_t is the random interference of the time-series, and B is the delay operator. For a time-series, $x_{t-1} = Bx_t, x_{t-2} = B^2x_t, \dots, x_{t-p} = B^p x_t$, for random interference, $\varepsilon_{t-1} = B\varepsilon_t, \varepsilon_{t-2} = B^2\varepsilon_t, \dots, \varepsilon_{t-q} = B^q \varepsilon_t$. $\Phi(B) = 1 - \phi_1 B - \phi_2 B^2 - \dots - \phi_p B^p$. $\Theta(B) = 1 - \theta_1 B - \theta_2 B^2 - \dots - \theta_q B^q$, p is the order of the auto-regressive model, q is the order of the moving average model, and d is the order of the difference.

The essence of DU-ARIMA model is the combination of the difference operation and dynamic updated-auto-regressive moving average (DU-ARMA) models. This means that any non-stationary series is stationary after one or more difference operations. Therefore, when using the DU-ARIMA model to predict the non-stationary sequence, firstly, the non-stationary sequence is transformed into a stationary sequence after a difference operation. Secondly, the DU-ARMA model is used to predict the stationary sequence. Finally, the non-stationary sequence-prediction value can be obtained by recovering the difference operation.

We let $y_t = (1 - B)^d x_t = \nabla^d x_t = \nabla^{d-1} x_t - \nabla^{d-1} x_{t-1} = \sum_{i=0}^d (-1)^d C_d^i x_{t-i}$, where $C_d^i = \frac{n!}{i!(d-i)!}$. After applying the above difference operation, Equation (1) can be transformed into the auto-regressive moving average (ARMA) model without considering the condition that x_{t+1} can be dynamically updated, which is expressed as

$$\Phi(B)y_t = \Theta(B)\varepsilon_t. \tag{2}$$

According to the stationarity and reversibility of the ARMA model, the ARMA process has both the infinite moving average representation $y_t = [\Phi(B)]^{-1}\Theta(B)\varepsilon_t = \Psi(B)\varepsilon_t$, and the infinite auto-regressive representation $\varepsilon_t = [\Theta(B)]^{-1}\Phi(B)y_t = \Pi(B)y_t$. For the infinite moving average representation, the time-series y_t can be represented by a linear function of random interference terms, see Equation (3). Then, the true value of the subsequent l time-steps of the time-series can be expressed by Equation (4).

$$y_t = [\Phi(B)]^{-1}\Theta(B)\varepsilon_t = \Psi(B)\varepsilon_t = \sum_{i=0}^{\infty} \varphi_i \varepsilon_{t-i}. \tag{3}$$

$$\begin{aligned} y_{t+l} &= \sum_{i=0}^{\infty} \varphi_i \varepsilon_{t+l-i} \\ &= \varphi_0 \varepsilon_{t+l} + \varphi_1 \varepsilon_{t+l-1} + \dots + \varphi_l \varepsilon_t + \varphi_{l+1} \varepsilon_{t-1} + \dots \\ &= \sum_{i=0}^{l-1} \varphi_i \varepsilon_{t+l-i} + \sum_{i=0}^{\infty} \varphi_{l+i} \varepsilon_{t-i}. \end{aligned} \tag{4}$$

Since $\varepsilon_{t+l}, \varepsilon_{t+l-1}, \dots, \varepsilon_{t+1}$ cannot be obtained, y_{t+l} can only be estimated by the linear combination of $\varepsilon_t, \varepsilon_{t-1}, \varepsilon_{t-2}, \dots$, denoted by \hat{y}_{t+l} , which is recorded as Equation (5). From this, the prediction error value of the ARMA model's infinite moving average representation can be obtained, see Equation (6) for details. Equation (7) is the variance of the prediction error for the ARMA model's infinite moving average representation.

$$\hat{y}_{t+l} = \sum_{i=0}^{\infty} D_i \varepsilon_{t-i}. \tag{5}$$

$$\begin{aligned}
 e_{t+l} &= y_{t+l} - \hat{y}_{t+l} \\
 &= \sum_{i=0}^{l-1} \varphi_i \varepsilon_{t+l-i} + \sum_{i=0}^{\infty} \varphi_{l+i} \varepsilon_{t-i} - \sum_{i=0}^{\infty} D_i \varepsilon_{t-i} \\
 &= \sum_{i=0}^{l-1} \varphi_i \varepsilon_{t+l-i} + \sum_{i=0}^{\infty} (\varphi_{l+i} - D_i) \varepsilon_{t-i}.
 \end{aligned} \tag{6}$$

$$\text{Var}(e_{t+l}) = \sum_{i=0}^{l-1} \varphi_i^2 \sigma_\varepsilon^2 + \sum_{i=0}^{\infty} (\varphi_{l+i} - D_i)^2 \sigma_\varepsilon^2. \tag{7}$$

Only when $\varphi_{l+i} = D_i$, is the value of the prediction error the smallest. At this time, \hat{y}_{t+l} , e_{t+l} and $\text{Var}(e_{t+l})$ can be expressed by Equation (8), Equation (9), and Equation (10), respectively.

$$\hat{y}_{t+l} = \sum_{i=0}^{\infty} \varphi_{l+i} \varepsilon_{t-i}. \tag{8}$$

$$e_{t+l} = \sum_{i=0}^{l-1} \varphi_i \varepsilon_{t+l-i}. \tag{9}$$

$$\text{Var}(e_{t+l}) = \sum_{i=0}^{l-1} \varphi_i^2 \sigma_\varepsilon^2. \tag{10}$$

For the dynamic updated-infinite moving average representation, considering the fact that the condition x_{t+1} can be dynamically updated to obtain (y_{t+1} also can be obtained by difference operation), $\varepsilon_{t+1} = y_{t+1} - \hat{y}_{t+1}$ is known. The estimated value of the subsequent l time-steps after the dynamic update can be expressed by Equation (11). The prediction error value after the dynamic update is shown in Equation (12). Equation (13) is the variance of the prediction error for the dynamic updated-infinite moving average representation.

$$\hat{y}'_{t+l} = \sum_{i=0}^{\infty} \varphi_{l+i-1} \varepsilon_{t-i+1}. \tag{11}$$

$$\begin{aligned}
 e'_{t+l} &= y_{t+l} - \hat{y}'_{t+l} \\
 &= \sum_{i=0}^{l-2} \varphi_i \varepsilon_{t+l-i} + \sum_{i=0}^{\infty} \varphi_{l+i-1} \varepsilon_{t-i+1} - \sum_{i=0}^{\infty} \varphi_{l+i-1} \varepsilon_{t-i+1} \\
 &= \sum_{i=0}^{l-2} \varphi_i \varepsilon_{t+l-i}.
 \end{aligned} \tag{12}$$

$$\text{Var}(e'_{t+l}) = \sum_{i=0}^{l-2} \varphi_i^2 \sigma_\varepsilon^2. \tag{13}$$

It is clear that the variance of the prediction error for a dynamic updated-infinite moving average representation Equation (13) is smaller than that of an ARMA's infinite moving average representation (Equation (10)) by $\varphi_{l-1}^2 \sigma_\varepsilon^2$.

The infinite auto-regressive representation $\varepsilon_t = [\Theta(B)]^{-1} \Phi(B) y_t = \Pi(B) y_t$ can be also expressed as

$$\varepsilon_t = [\Theta(B)]^{-1} \Phi(B) y_t = \Pi(B) y_t = \sum_{j=0}^{\infty} \pi_j y_{t-j} \tag{14}$$

or

$$y_t = \varepsilon_t + \sum_{j=1}^{\infty} \pi_j y_{t-j}. \tag{15}$$

It can be seen from Equation (15) that the essence of infinite auto-regressive representation is to predict y_{t+l} by the known historical data, $y_t, y_{t-1}, y_{t-2}, \dots$. It is easy to draw the conclusions that: if the predicted time-step l is longer, the more unknown data there will be, and the lower the accuracy of data prediction will be. However, for the dynamic updated-infinite auto-regressive representation, it can continuously obtain new monitoring data, y_{t+1}, y_{t+2}, \dots , based on the original historical data $y_t, y_{t-1}, y_{t-2}, \dots$. This means that the number of unknown data is reduced, which can improve the prediction accuracy of y_{t+l} . The variance of the prediction error for a dynamic updated-infinite auto-regressive representation is smaller than that of an infinite auto-regressive representation by $\pi_{l-1}^2 \text{Var}(y_{t+1})$ (similar to the variance of the prediction error for a dynamic updated-infinite moving average representation, see Appendix A for details).

The DU-ARMA model can be seen as a combination of the dynamic updated-infinite moving average representation and the dynamic updated-infinite auto-regressive representation, so the variance of the prediction error of the DU-ARMA model is smaller than that of the ARMA model. According to the difference relationship between DU-ARMA and DU-ARIMA, the DU-ARIMA model obtained after the recovery difference operation can predict the non-stationary sequence, and the variance of the prediction error of DU-ARIMA model is also smaller than that of the ARIMA model. The essence of the DU-ARIMA model is to input the current monitoring data into the ARIMA model in real time to realize the dynamic update of historical data. The term “dynamic updated” in DU-ARIMA means that the user can access the real value of the current time-step to update the model before predicting the next time-step. Therefore, DU-ARIMA can effectively improve the accuracy of data prediction. The quality of the DU-ARIMA prediction result can be measured by the root mean square error (RMSE). The smaller the RMSE value, the better the DU-ARIMA prediction result.

2.3. Multiple Isolation Forest

For the difficulty of obtaining degradation malfunction samples, the multiple isolation forest (M-iForest) model is selected to predict the degradation malfunction of historical monitoring data and predicted data. To know what M-iForest is, it is necessary to start with isolation forest. Isolation forest is an effective unsupervised outlier detection model [29]. Its main idea is that outliers are few and different.

If isolation forest alone is used to predict the degradation malfunction, there are two main processes. Firstly, the historical monitoring data and predicted data are randomly sampled to construct an isolation binary tree. Secondly, the malfunction score of each data point is obtained through the isolation forest established by the isolation binary tree. The specific process is shown in part 1 inside the dashed box of Figure 2. To solve the problems of swamping (normal samples are recognized as outliers) and masking (too many outliers to cover up the existence of abnormality) caused by too much data, multiple isolation binary trees are constructed by random sub-sampling. However, the formation of binary trees is random, which makes it unreliable for a single isolation binary tree to find outliers using shorter paths. Therefore, multiple isolation binary trees are formed into an isolation forest to improve reliability. For any sample, x , the malfunction score can be calculated using Equations (16)–(18), where $s(x, n)$ is the malfunction score, $E[h(x)]$ is the average value of the sample x path length $h(x)$ in a set of isolation trees, $c(n)$ is the average path length of the unsuccessful search in the isolation binary tree for the given n samples, $H(k)$ is the number of harmonics, and ζ is Euler’s constant. The calculated malfunction score, s , is in the range of $[0, 1]$. If s is closer to 1, it means that the sample is more likely to be a degradation malfunction sample. Conversely, if s is closer to 0, it indicates that the sample is more likely to be a normal sample.

$$s(x, n) = 2^{-\frac{E[h(x)]}{c(n)}}. \quad (16)$$

$$c(n) = 2H(n-1) - \frac{2(n-1)}{n}. \quad (17)$$

$$H(k) = \ln(k) + \zeta. \quad (18)$$

To further improve the reliability and stability of isolation forest, an M-iForest model is proposed, which aims to construct many isolation forests to ensure the stability of the malfunction prediction and evaluate the model, as shown in Figure 2 for a whole model. The generalizability and stability of the model can be evaluated by the area under curve (AUC). The model will obtain multiple AUC values, because of the construction of multiple rounds of isolation forests. If the average of AUC is closer to 1, the better the model effect

and the stronger the generalization ability, while the smaller the variance of AUC, the better the stability of the model.

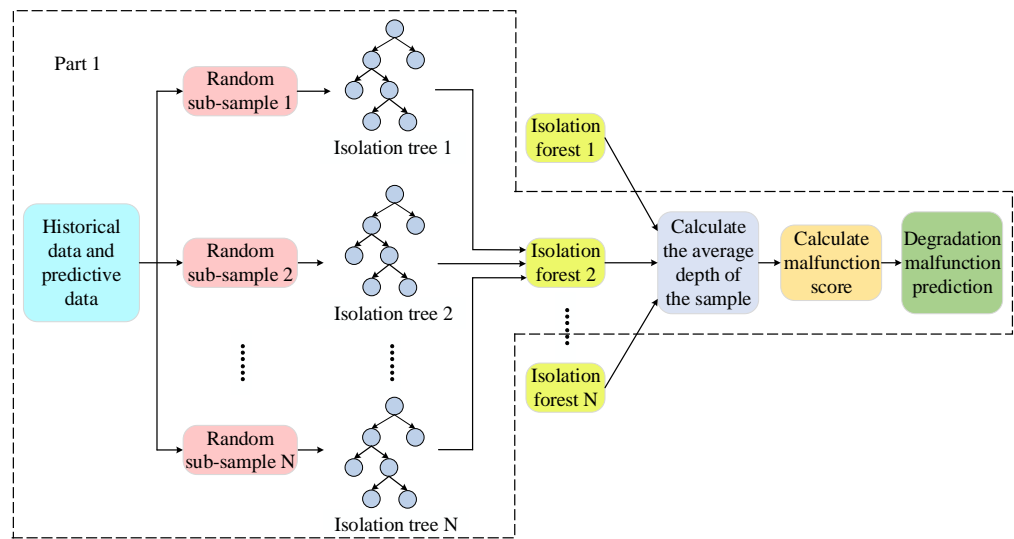


Figure 2. M-iForest flow chart.

3. Experiment and Analysis

3.1. Experimental Conditions and Experimental Design

The experimental platform is a certain type of marine radar transmitter, and multiple microwave measurement points can be set on the transmitter to monitor the historical working data of the radar transmitter before any degradation malfunction. To achieve the purpose of visualization of the experimental results, the experiment collected historical data of two microwave measurement points (peak power and operating frequency) to verify the feasibility and portability of the model. The data-sampling frequency of the two monitoring points is 1 time per 10 min. The hard-wired settings of the experiment are shown in Figure 3.

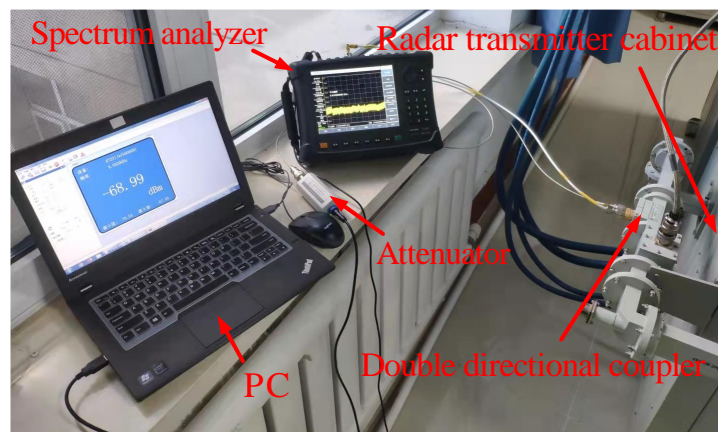


Figure 3. The hard-wired settings of the experiment.

To verify the feasibility and portability of the proposed prognostic model, the experiment collects two different historical monitoring data concerning the degradation malfunction of the radar transmitter. Each monitoring point of the first type of degradation malfunction provides 192 historical data, and the degradation malfunction occurs at the 193rd time-step. The monitoring data of the first type of degradation malfunction after wavelet denoising is shown in Figure 4. A total of 253 historical data were recorded for the second type of degradation malfunction, and the second type of degradation malfunction

occurred at the 254th time-step. The monitoring data after denoising are shown in Figure 5. Experimental data processing and prognostic algorithms were conducted on the MATLAB 2019b platform.

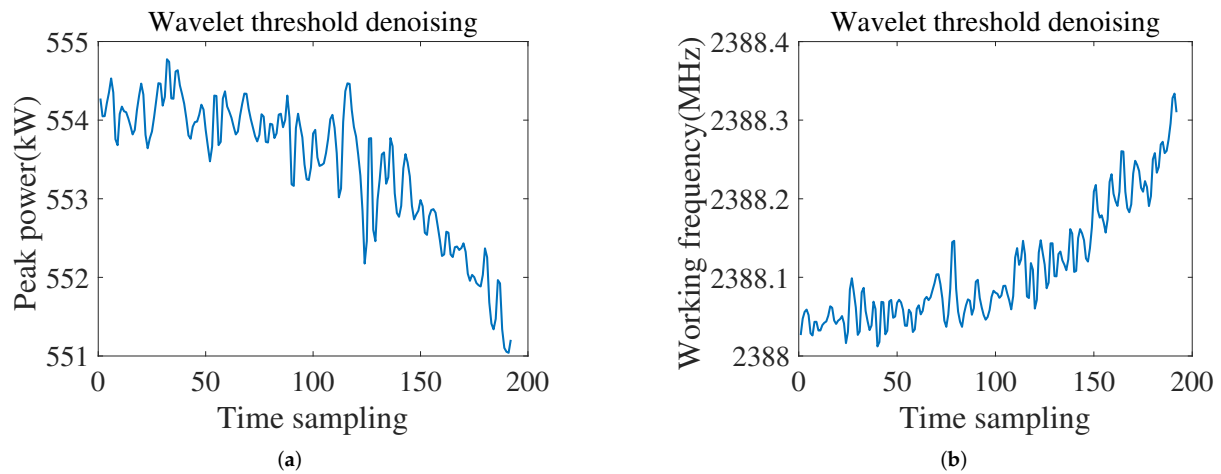


Figure 4. The monitoring data after denoising of the first type of degradation malfunction. (a) Peak power. (b) Working frequency.

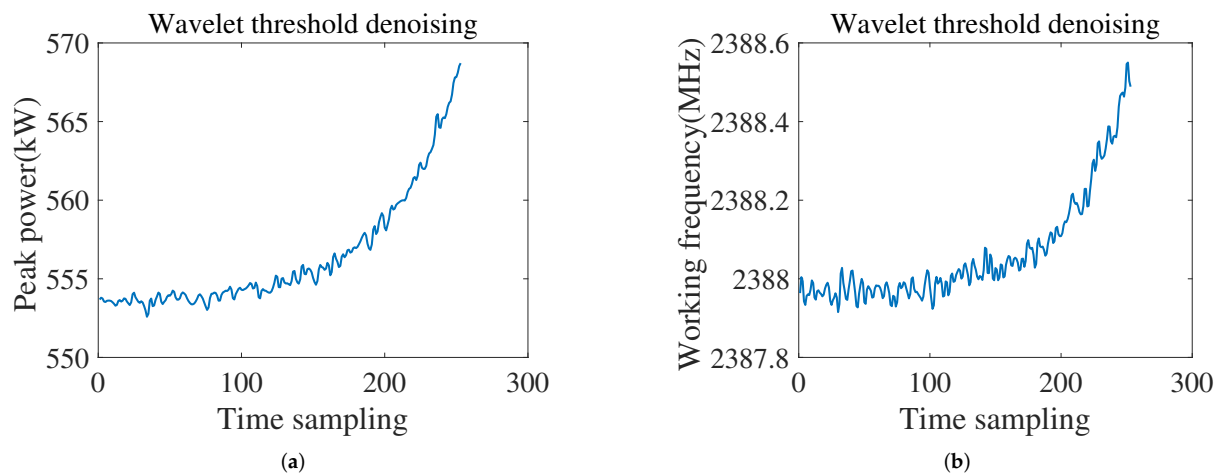


Figure 5. The monitoring data after denoising of the second type of degradation malfunction. (a) Peak power. (b) Working frequency.

3.2. Feasibility Experiment and Result Analysis

To verify the feasibility and validity of the proposed model, the first type of degradation malfunction data is selected for the experiment. The first 90% (173) of the denoising data is selected as the historical data. ADF and KPSS are used for the stationarity test. The return value and stationarity results of the test are shown in Table 2. It can be seen from the table that the two historical data are non-stationary series, so DU-ARIMA needs to be used to predict the data of the next 10% (19). The DU-ARIMA(1,1,10) model should be used for the data prediction of peak power and the DU-ARIMA(3,1,13) model for operating frequency. To obtain more accurate data prediction results, we set the prediction time-step $l = 1$. The prediction results are shown in Figure 6. The predicted data are compared with the real monitoring data, and the RMSE is calculated to evaluate the DU-ARIMA model. Partial magnifications of the prediction result and RMSE are shown in Figure 7. It can be seen from the figure that the RMSE of the two microwave measurement points predicted by DU-ARIMA are 0.068333 and 0.0077417, respectively, which are much lower than the

0.15848 and 0.028292 in [21]. The experiment results show that the DU-ARIMA has higher a prediction accuracy.

Table 2. Test results of stationarity for measurement data of the first type of degradation malfunction.

The Historical Data	ADF	KPSS	Stationarity
Peak power	0	1	Non-stationarity
Operating frequency	0	1	Non-stationarity

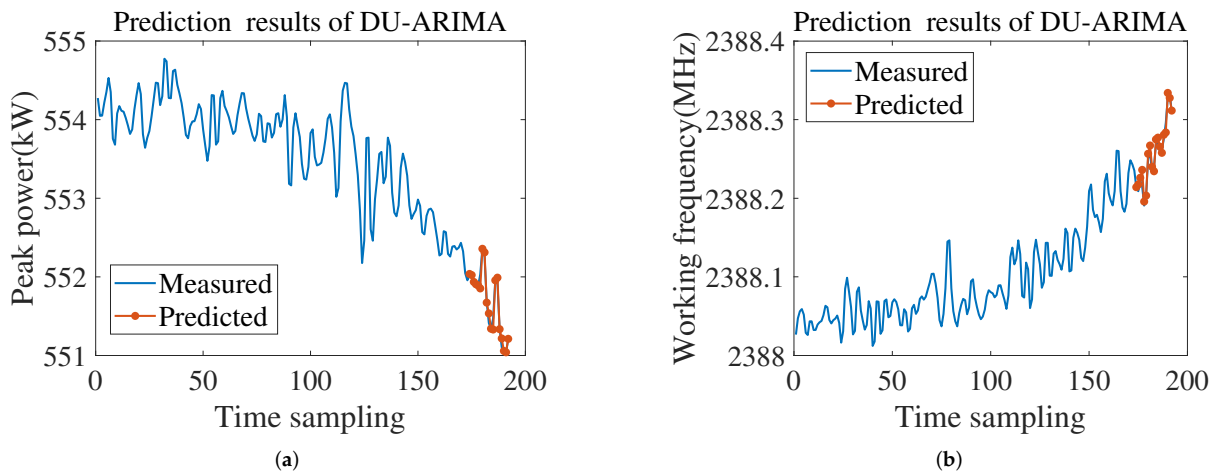


Figure 6. Monitoring data after denoising and prediction results of the first type of degradation malfunction. (a) Peak power. (b) Working frequency.

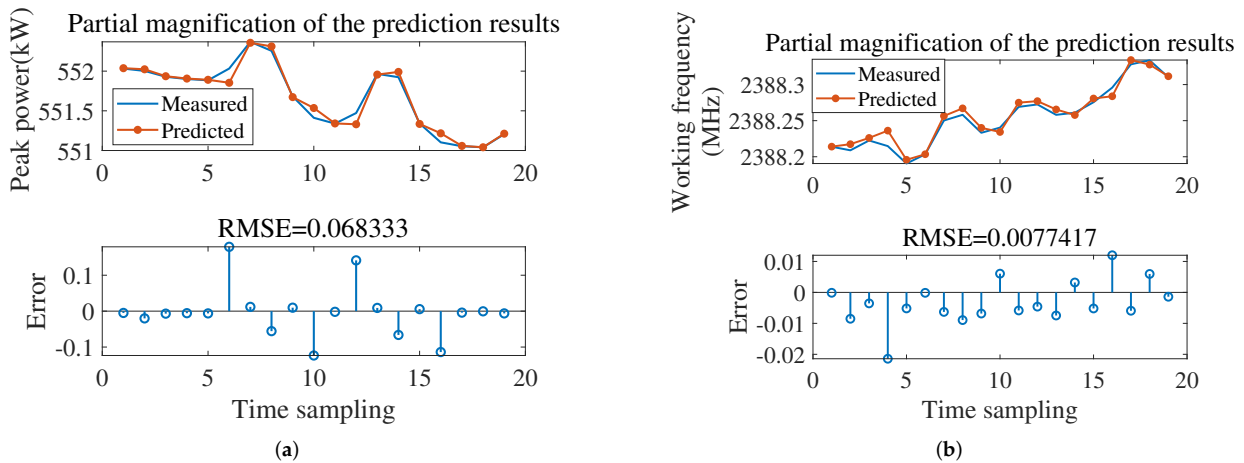


Figure 7. Partial magnification of prediction results and RMSE of the first type of degradation malfunction. (a) Peak power. (b) Working frequency.

It can be considered that the predicted data can represent the actual data on the basis of DU-ARIMA’s accurate prediction of the data. At this time, the unsupervised M-iForest model is used to detect the degradation malfunction for the historical data and the prediction data of the two measurement points (peak power and operating frequency). In the experiment, the number of random sub-sampling is 256, the number of isolated binary trees is 100, and the number of isolation forests is 10. The model provides the alarm time-step for the degradation malfunction and uses AUC to evaluate the model. The experimental results are shown in Table 3. It can be seen from the table that the average of the AUC is 0.9895 (close to 1), which means that the model has a strong generalizability. The variance of AUC is 0, that is, the model is stable. The earliest alarm time-step is 183. This

indicates that the M-iForest model can predict the degradation malfunction 10 time-steps (100 min) in advance. Since the two-dimensional data has the characteristic of visualization, the visualization results of the experiment are shown in Figure 8. The samples marked by the green circles in the Figure 8 are the malfunction alarm samples detected by M-iForest. Obviously, these samples are more alienated from other samples, so they are more likely to be detected as malfunction samples.

Table 3. M-iForest model evaluation results and malfunction alarm time-step of the first type of degradation malfunction.

The Evaluation Results	Values
AUC Average	0.9895
AUC Variance	0
Alarm time-step	183, 184, 188, 189, 190, 191, 192

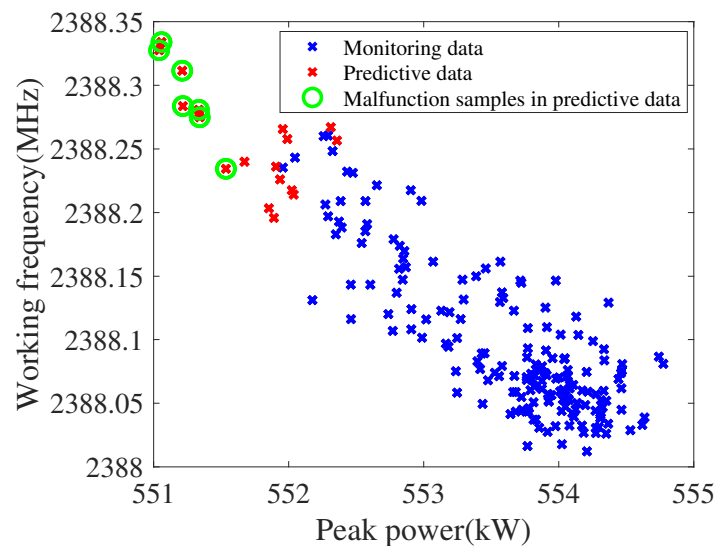


Figure 8. The visualization results of the first type of degradation malfunction prognosis experiment.

The result of the M-iForest degradation malfunction detection without prediction by DU-ARIMA are shown in Table 4 and Figure 9. Compared with Table 3, we find that the alarm time-step is not much different, but the alarm time differs by one data-sampling time interval. For example, a malfunction alarm will occur at the time-step 183 identically, and the M-iForest alarm time with prediction by DU-ARIMA will be one data-sampling interval earlier than that of the alarm time without prediction by DU-ARIMA (10 min). Specifically, the M-iForest malfunction detection with prediction by DU-ARIMA is to predict and alarm for the 183rd time-step when the 182nd monitoring data point is obtained, while the M-iForest malfunction detection without DU-ARIMA will sound an alarm after 10 min (after obtaining the 183rd monitoring data). For a large and complex electronic device such as radar, this precious 10 min will avoid a lot of unnecessary losses. Therefore, if the data-sampling time interval is longer, the malfunction alarm time with prediction by DU-ARIMA will be earlier than the alarm time without prediction by DU-ARIMA.

Table 4. M-iForest model evaluation results and malfunction alarm time-step without prediction by DU-ARIMA.

The Evaluation Results	Values
AUC Average	0.9906
AUC Variance	0.0022
Alarm time-step	183, 184, 185, 188, 189, 190, 191, 192

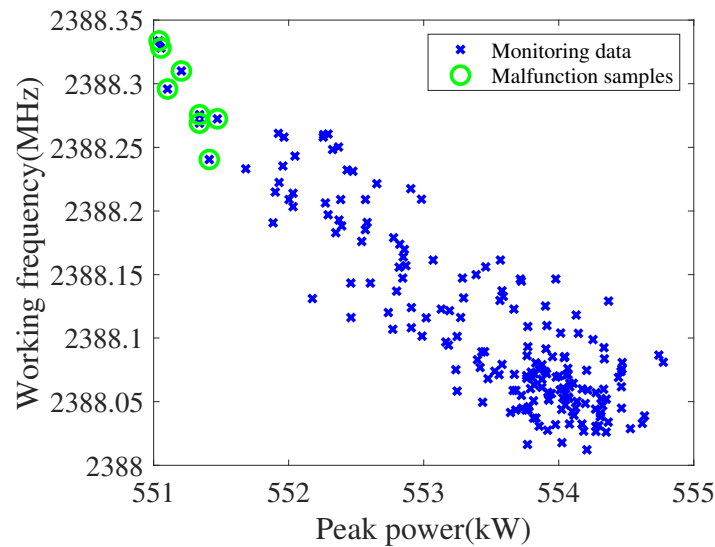


Figure 9. The visualization results of the degradation malfunction prognosis experiment without prediction by DU-ARIMA.

The experimental results for the first type of degradation malfunction show that the novel prognostic model for radar transmitter degradation malfunction combined with DU-ARIMA and M-iForest proposed in this paper is reasonable and feasible.

3.3. Portability Experiment and Result Analysis

To verify the portability of the proposed model, the second type of degradation malfunction data is selected for the same experiment with the same method. Among them, the first 90% (229) of the denoising data was used for testing the stationarity by ADF and KPSS. As expected, the data of the two microwave measurement points are non-stationary series. So, the next 10% (25) of the data can be predicted by DU-ARIMA, the DU-ARIMA(13, 1, 14) model for the data prediction of peak power, and the DU-ARIMA(6, 1, 14) model for operating frequency. The partial magnification of the prediction result and RMSE are shown in Figure 10. At the same time, the unsupervised M-iForest model completes the degradation malfunction detection for the 229 historical data and 25 predicted data. The M-iForest model evaluation results and malfunction alarm time-step of the second type of degradation malfunction are shown in Table 5. The visualization results of the second type of degradation malfunction prognosis experiment are shown in Figure 11.

Table 5. M-iForest model evaluation results and malfunction alarm time-step of the second type of degradation malfunction.

The Evaluation Results	Values
AUC Average	0.9944
AUC Variance	0.0028
Alarm time-step	244, 245, 246, 247, 248, 249, 250, 251, 252, 253

It can be seen from the results of the portability experiment that the RMSE of the prediction results for the peak power and the operating frequency in Figure 10 are 0.12995 and 0.0079966, respectively. The earliest alarm time-step in Table 5 is 244, that is, the proposed method can predict the degradation malfunction 10 time-steps (100 min) in advance. The visualization results in Figure 11 are similar to those in Figure 8. The samples marked with green circles are alienated from other samples and are the degradation fault alarm samples detected by M-iForest. It is clear that the proposed model has good portability and can be applied to the prediction of different types of degradation malfunction.

Table 6 compares the proposed degradation malfunction prognostic model with the previous method. It can be seen from the table that, compared with [19–21], the method proposed in this paper has a smaller sample size. It also does not need to set the artificial threshold, extract the feature, and use the fault samples for training.

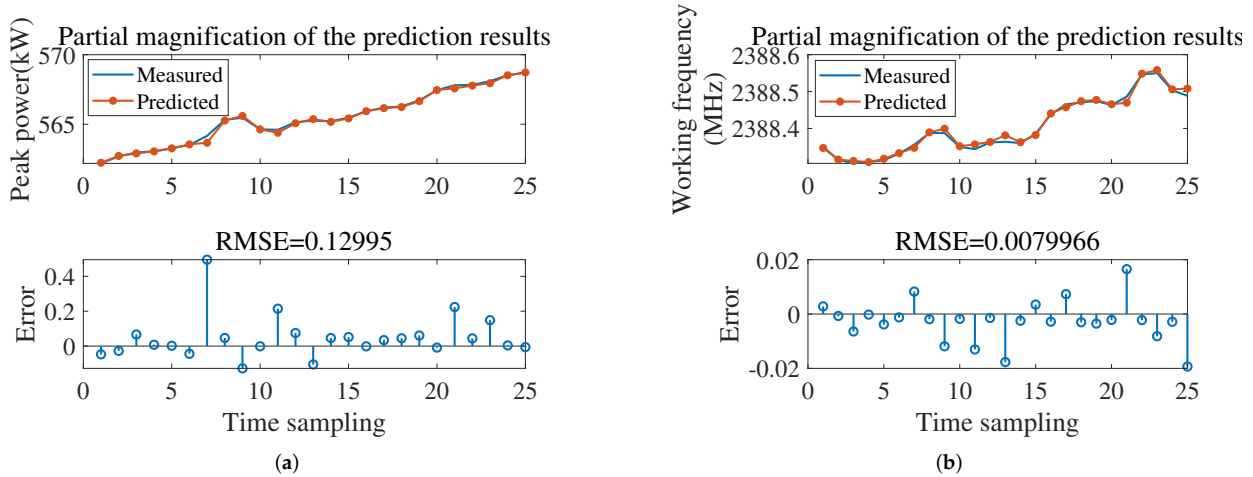


Figure 10. Partial magnification of prediction results and RMSE of the second type of degradation malfunction. (a) Peak power. (b) Working frequency.

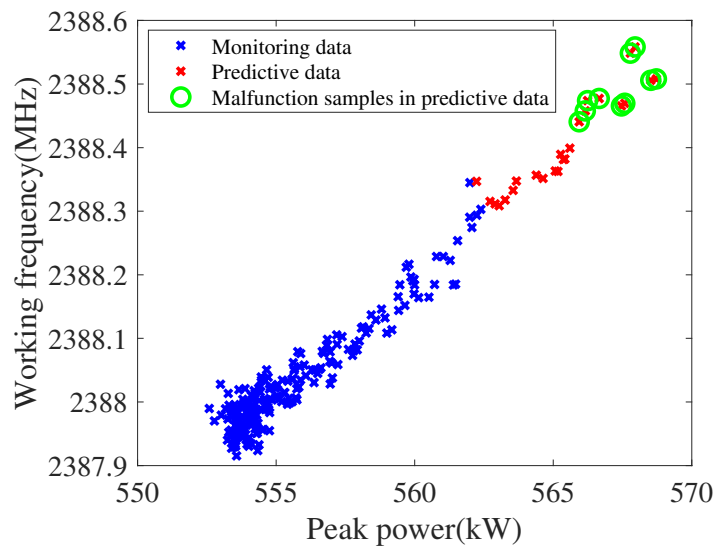


Figure 11. Visualization results of the second type of degradation malfunction prognosis experiment.

Table 6. Comparison between the proposed method and the existing method.

Reference	[19]	[20]	[21]	This Work
Artificial threshold	Yes	No	No	No
Feature extraction	Yes	No	No	No
The historical data	1120	5500	<300	<300
The fault sample	Not mentioned	Not mentioned	≥1	No need

4. Conclusions

This paper proposed a novel radar transmitter degradation malfunction prognosis model that combined with DU-ARIMA and M-iForest. This method considers the restrictions of the difficulty in obtaining fault samples and the fact that monitoring data cannot reach the fault threshold. This paper discusses the workflow and basic theory of

the proposed prognostic model for radar transmitter degradation fault. We set up two microwave measurement points and different types of degradation malfunction experiments to verify the feasibility and portability of the model. The degradation malfunction can be predicted at least 10 time-steps (100 min) before its occurrence. Compared with existing radar degradation malfunction prediction methods, the proposed method can complete the degradation malfunction prognosis using less historical data, no artificial thresholds, no features extraction, and no fault samples. The experimental results show that the model can effectively and feasibly realize the prediction of degradation malfunctions for radar transmitters.

Author Contributions: Conceptualization, Y.Z. and S.F.; methodology, Y.Z. and D.L.; software, Y.Z.; data curation, Z.C.; writing—original draft preparation, Y.Z.; writing—review and editing, Y.Z., S.F., D.L. and Z.C.; visualization, Y.Z. All authors have read and agreed to the published version of this manuscript.

Funding: This research was funded by the National Natural Science Foundation of China (No.51809030).

Acknowledgments: The equipment and data used in the analyses were provided by the Department of Information Systems, Dalian Naval Academy.

Conflicts of Interest: The authors declare no conflict of interest.

Abbreviations

The following abbreviations are used in this manuscript:

BIT	Built-In Test
MIMO	Multiple-Input–Multiple-Output
LSTM	Long Short-Term Memory
DU-ARIMA	Dynamic Updated-Auto-Regressive Integrated Moving Average
M-iForest	Multiple-isolation Forest
ADF	Augmented Dickey–Fuller
KPSS	Kwiatkowski–Phillips–Schmidt–Shin
ARIMA	Auto-Regressive Integrated Moving Average
DU-ARMA	Dynamic Updated-Auto-Regressive Moving Average
ARMA	Auto-Regressive Moving Average
RMSE	Root Mean Square Error
M-iForest	Multiple isolation Forest
AUC	Area Under Curve

Appendix A

The infinite auto-regressive representation $\varepsilon_t = [\Theta(B)]^{-1}\Phi(B)y_t = \Pi(B)y_t$, can be also expressed as

$$\varepsilon_t = [\Theta(B)]^{-1}\Phi(B)y_t = \Pi(B)y_t = \sum_{j=0}^{\infty} \pi_j y_{t-j} \quad (A1)$$

or

$$y_t = \varepsilon_t + \sum_{j=1}^{\infty} \pi_j y_{t-j}. \quad (A2)$$

The true value of the subsequent l time-steps of the time-series can be expressed by

$$\begin{aligned} y_{t+l} &= \varepsilon_{t+l} + \sum_{j=1}^{\infty} \pi_j y_{t+l-j} \\ &= \varepsilon_{t+l} + \sum_{j=1}^{l-1} \pi_j y_{t+l-j} + \sum_{j=0}^{\infty} \pi_{l+j} y_{t-j} \\ &= \varepsilon_{t+l} + \sum_{j=1}^l \pi_j y_{t+l-j} + \sum_{j=1}^{\infty} \pi_{l+j} y_{t-j}. \end{aligned} \quad (A3)$$

Since y_{t+l} can only be estimated by the linear combination of $y_t, y_{t-1}, y_{t-2}, \dots$, denoted by \hat{y}_{t+l} , which is recorded as

$$\hat{y}_{t+l} = \varepsilon_t + \sum_{j=0}^{\infty} E_j y_{t-j}. \tag{A4}$$

From this, the prediction error value of the ARMA's infinite auto-regressive representation can be obtained by

$$\begin{aligned} f_{t+l} &= y_{t+l} - \hat{y}_{t+l} \\ &= \varepsilon_{t+1} - \varepsilon_t + \sum_{j=1}^{l-1} \pi_j y_{t+l-j} + \sum_{j=0}^{\infty} (\pi_{l+j} - E_j) y_{t-j}, \end{aligned} \tag{A5}$$

only when $\pi_{l+j} = E_j$, the value of the prediction error is the smallest. So, \hat{y}_{t+l}, f_{t+l} and $\text{Var}(f_{t+l})$ can, respectively, be expressed by

$$\hat{y}_{t+l} = \varepsilon_t + \sum_{j=0}^{\infty} \pi_{l+j} y_{t-j}. \tag{A6}$$

$$f_{t+l} = \varepsilon_{t+1} - \varepsilon_t + \sum_{j=1}^{l-1} \pi_j y_{t+l-j}. \tag{A7}$$

$$\begin{aligned} \text{Var}(f_{t+l}) &= \text{Var}(\varepsilon_{t+1}) - \text{Var}(\varepsilon_t) + \text{Var}\left(\sum_{j=1}^{l-1} \pi_j y_{t+l-j}\right) \\ &= \sigma_{\varepsilon}^2 - \sigma_{\varepsilon}^2 + \sum_{j=1}^{l-1} \pi_j^2 \text{Var}(y_{t+l-j}) \\ &= \sum_{j=1}^{l-1} \pi_j^2 \text{Var}(y_{t+l-j}). \end{aligned} \tag{A8}$$

For the dynamic updated infinite auto-regressive representation, considering the fact that the condition x_{t+1} can be dynamically updated to obtain y_{t+1} , i.e., it can also be obtained by a difference operation. The estimated value of the subsequent l time-steps after the dynamic update can be expressed by

$$\begin{aligned} \hat{y}'_{t+l} &= \varepsilon_t + \sum_{j=0}^{\infty} \pi_{l+j-1} y_{t-j+1} \\ &= \varepsilon_t + \sum_{j=l-1}^l \pi_j y_{t+l-j} + \sum_{j=1}^{\infty} \pi_{l+j} y_{t-j}. \end{aligned} \tag{A9}$$

The prediction error value of ARMA's dynamic updated infinite auto-regressive representation can be obtained by

$$\begin{aligned} f'_{t+l} &= y_{t+l} - \hat{y}'_{t+l} \\ &= \varepsilon_{t+1} - \varepsilon_t + \sum_{j=1}^l \pi_j y_{t+l-j} - \sum_{j=l-1}^l \pi_j y_{t+l-j} \\ &= \varepsilon_{t+1} - \varepsilon_t + \sum_{j=1}^{l-2} \pi_j y_{t+l-j}. \end{aligned} \tag{A10}$$

The variance of the prediction error for the dynamic updated infinite auto-regressive representation can be expressed as

$$\begin{aligned} \text{Var}(f'_{t+l}) &= \text{Var}(\varepsilon_{t+1}) - \text{Var}(\varepsilon_t) + \text{Var}\left(\sum_{j=1}^{l-2} \pi_j y_{t+l-j}\right) \\ &= \sigma_{\varepsilon}^2 - \sigma_{\varepsilon}^2 + \sum_{j=1}^{l-2} \pi_j^2 \text{Var}(y_{t+l-j}) \\ &= \sum_{j=1}^{l-2} \pi_j^2 \text{Var}(y_{t+l-j}). \end{aligned} \tag{A11}$$

It is clear that the variance of the prediction error for a dynamic updated infinite auto-regressive representation is smaller than that of an infinite auto-regressive representation by $\pi_{l-1}^2 \text{Var}(y_{t+1})$.

References

1. Cui, Z.; Henrickson, K.; Ke, R.; Wang, Y. Traffic graph convolutional recurrent neural network: A Deep Learning framework for network-scale traffic learning and forecasting. *IEEE Trans. Intell. Transp. Syst.* **2020**, *21*, 4883–4894. [[CrossRef](#)]
2. Zhu, J.; Li, S.; Liu, Y.; Dong, H. A Hybrid Method for the Fault Diagnosis of Onboard Traction Transformers. *Electronics* **2022**, *11*, 762. [[CrossRef](#)]
3. Ghanim, M.S.; Abu-Lebdeh, G. Projected state-wide traffic forecast parameters using artificial neural networks. *IET Intell. Transp. Syst.* **2019**, *13*, 661–669. [[CrossRef](#)]
4. Zhang, J.; Du, D.; Bao, Y.; Wang, J.; Wei, Z. Development of multifrequency-swept microwave sensing system for moisture measurement of sweet corn with deep neural network. *IEEE Trans. Instrum. Meas.* **2020**, *69*, 6446–6454. [[CrossRef](#)]
5. Nabulsi, A.A.; Al-Shaikhli, W.; Kettlewell, C.; Hejtmanek, K.; Hassan, A.M.; Derakhshani, R. Machine Learning Classification of S-Band Microwave Scattering Measurements From the Forearm as a Novel Biometric Technique. *IEEE Open J. Antennas Propag.* **2020**, *1*, 118–125. [[CrossRef](#)]
6. Huang, N.; Chen, Q.; Cai, G.; Xu, D.; Zhang, L.; Zhao, W. Fault diagnosis of bearing in wind turbine gearbox under actual operating conditions driven by limited data with noise labels. *IEEE Trans. Instrum. Meas.* **2020**, *70*, 1–10. [[CrossRef](#)]
7. Lin, S.L. Application of Machine Learning to a Medium Gaussian Support Vector Machine in the Diagnosis of Motor Bearing Faults. *Electronics* **2021**, *10*, 2266. [[CrossRef](#)]
8. Long, J.; Zhang, S.; Li, C. Evolving deep echo state networks for intelligent fault diagnosis. *IEEE Trans. Ind. Inform.* **2019**, *16*, 4928–4937. [[CrossRef](#)]
9. Dong, G.; Yang, F.; Wei, Z.; Wei, J.; Tsui, K.L. Data-driven battery health prognosis using adaptive brownian motion model. *IEEE Trans. Ind. Inform.* **2020**, *16*, 4736–4746. [[CrossRef](#)]
10. El Mejdoubi, A.; Chaoui, H.; Gualous, H.; Van Den Bossche, P.; Omar, N.; Van Mierlo, J. Lithium-ion batteries health prognosis considering aging conditions. *IEEE Trans. Power Electron.* **2019**, *34*, 6834–6844. [[CrossRef](#)]
11. Hu, X.; Che, Y.; Lin, X.; Deng, Z. Health prognosis for electric vehicle battery packs: A data-driven approach. *IEEE-ASME Trans. Mechatron.* **2020**, *25*, 2622–2632. [[CrossRef](#)]
12. Yang, R.; Yu, L.; Zhao, Y.; Yu, H.; Xu, G.; Wu, Y.; Liu, Z. Big data analytics for financial market volatility forecast based on support vector machine. *Int. J. Inf. Manag.* **2020**, *50*, 452–462. [[CrossRef](#)]
13. Ren, R.; Wu, D.D.; Liu, T. Forecasting stock market movement direction using sentiment analysis and support vector machine. *IEEE Syst. J.* **2018**, *13*, 760–770. [[CrossRef](#)]
14. Chou, J.S.; Nguyen, T.K. Forward forecast of stock price using sliding-window metaheuristic-optimized machine-learning regression. *IEEE Trans. Ind. Inform.* **2018**, *14*, 3132–3142. [[CrossRef](#)]
15. Zhang, T.; Chen, J.; Chen, X. Array diagnosis using signal subspace clustering in MIMO radar. *Electron. Lett.* **2020**, *56*, 99–101. [[CrossRef](#)]
16. Khan, S.U.; Rahim, M.; Murad, N.; Zubir, F.; Ayop, O.; Yusoff, M.; Hamid, M.; Dewan, R. Detection of the Faulty Sensors on Basis of the Pattern Using Symmetrical Structure of Linear Array Antenna. *Appl. Comput. Electromagn. Soc. J.* **2017**, *32*, 358–365.
17. Chen, J.; Zhuo, Q.; Li, J.; Zhu, Y. Array diagnosis and angle estimation in bistatic MIMO radar under array antenna failures. *IET Radar Sonar Navig.* **2019**, *13*, 1180–1188. [[CrossRef](#)]
18. Finchera, D.; Migliore, M.D.; Lucido, M.; Schettino, F.; Panariello, G. Online failure detection in large massive MIMO linear arrays. In Proceedings of the 2017 International Applied Computational Electromagnetics Society Symposium-Italy (ACES), Florence, Italy, 26–30 March 2017; pp. 1–2.
19. Qianqian, L.; Jingyuan, Z.; Bing, C. Study on life prediction of radar based on non-parametric regression model. In Proceedings of the 2017 13th IEEE International Conference on Electronic Measurement & Instruments (ICEMI), Yangzhou, China, 20–22 October 2017; pp. 586–590.
20. Li, W.; Zhou, W.; Wang, Y.M.; Shen, C.; Zhang, X.; Li, X. Meteorological radar fault diagnosis based on deep learning. In Proceedings of the 2019 International Conference on Meteorology Observations (ICMO), Chengdu, China, 28–31 December 2019; pp. 1–4.
21. Zhai, Y.; Fang, S. A Degradation Fault Prognostic Method of Radar Transmitter Combining Multivariate Long Short-Term Memory Network and Multivariate Gaussian Distribution. *IEEE Access* **2020**, *8*, 199781–199791. [[CrossRef](#)]
22. Wang, C.; Lu, N.; Chen, Y.; Yu, H. A Data-driven Fault Detection Method for Radar Cooling System. In Proceedings of the 2021 CAA Symposium on Fault Detection, Supervision, and Safety for Technical Processes (SAFEPROCESS), Chengdu, China, 6–8 August 2021; pp. 1–5.
23. Li, Y.; Yang, J.; Fei, T.; Xie, Y. Few-shot Classification of Radar Equipment Fault Based on TF-IDF Feature Date Augmentation and BERT. In Proceedings of the 2021 International Conference on Machine Learning and Intelligent Systems Engineering (MLISE), Chongqing, China, 9–11 July 2021; pp. 444–448.
24. Zhao, G.; Liu, C.; Li, S.; Tian, Z.; Liu, X.; Li, H. Radar System Testability Design and Demonstration Based on Fault Modes and Software Control. In Proceedings of the 2021 8th International Conference on Dependable Systems and Their Applications (DSA), Yinchuan, China, 11–12 September 2021; pp. 307–314.
25. Mallat, S.; Hwang, W.L. Singularity detection and processing with wavelets. *IEEE Trans. Inf. Theory* **1992**, *38*, 617–643. [[CrossRef](#)]
26. Dickey, D.A.; Fuller, W.A. Distribution of the estimators for auto-regressive time series with a unit root. *J. Am. Stat. Assoc.* **1979**, *74*, 427–431.

27. Kwaitkowski, D.; Phillips, P.C.; Schmidt, P.; Shin, Y. Testing the null hypothesis of stationarity against the alternative of a unit root. *J. Econom.* **1992**, *54*, 159–178. [[CrossRef](#)]
28. Box, G.E.; Jenkins, G.M.; Reinsel, G.C.; Ljung, G.M. *Time Series Analysis: Forecasting and Control*; John Wiley & Sons, Inc.: Hoboken, NJ, USA, 2015.
29. Liu, F.T.; Ting, K.M.; Zhou, Z.H. Isolation forest. In Proceedings of the 2008 Eighth IEEE International Conference on Data Mining, Pisa, Italy, 15–19 December 2008; pp. 413–422.